

# Phase transition and electrical properties of $\text{Ni}_{1-x}\text{Zn}_x\text{Mn}_2\text{O}_4$ ( $0 \leq x \leq 1.0$ ) NTC ceramics

Fei Cheng · Junhua Wang · Huimin Zhang ·  
Aimin Chang · Wenwen Kong · Bo Zhang ·  
Long Chen

Received: 31 August 2014 / Accepted: 24 November 2014 / Published online: 3 December 2014  
© Springer Science+Business Media New York 2014

**Abstract** The  $\text{Ni}_{1-x}\text{Zn}_x\text{Mn}_2\text{O}_4$  ( $0 \leq x \leq 1.0$ ) negative temperature coefficient (NTC) ceramics were prepared by the traditional solid state reaction method. X-ray diffraction results show that the as-sintered ceramics transformed to tetragonal spinel ( $x = 1$ ) gradually from cubic spinel ( $x = 0$ ). Scanning electron microscope images show that the shape of grains changed with increasing Zn ions content, because of the stress in grains induced by phase transition. The resistivity decreased slightly with increasing Zn ions content for  $x \leq 0.25$ , but increased remarkably for higher Zn ions content. The values of  $\rho_{25}$ ,  $B_{25/50}$  and activation energy for  $\text{Ni}_{1-x}\text{Zn}_x\text{Mn}_2\text{O}_4$  ( $0 \leq x \leq 0.8$ ) NTC thermistors were in the range of 3,511–136,780  $\Omega$  cm, 3,913–4,491 K and 0.3271–0.3691 eV, respectively. The values of relative resistance drift  $\Delta R/R_0$  ( $0 \leq x \leq 0.8$ ) were  $< 2\%$  and had a minimum of 0.69 %, after aging test for 500 h. According to the complex impedance analysis, both of the NTC characteristic ( $0 \leq x \leq 1.0$ ) and the increase of resistivity with adding Zn ions content ( $x > 0.25$ ), were attributed to the increase of grain boundaries resistance.

## 1 Introduction

The negative temperature coefficient (NTC) ceramics have been widely used for temperature measurement, compensation, and infrared detections etc. [1–3], whose resistivity decreases exponentially with increasing temperature. Because of the broad applications, wide range and high stability of resistivity and  $B$  constant are desired. At present, most of the commercial oxide NTC thermistors are spinel [4–7] or perovskite [8, 9] structures. Besides,  $\text{NiMn}_2\text{O}_4$  system is one of the most studied spinel for NTC thermistors, and many researches have focused on improving its electrical properties [10, 11]. The characteristics of NTC thermistors can vary significantly with different compositions.

Substituting by other elements is an effective way to adjust the properties of NTC ceramics [12, 13]. In addition, effects of substituting have been studied in  $\text{Ni}_{1-x}\text{Mn}_{2+x}\text{O}_4$  system. For example, Fe (or Al) can be added to achieve higher  $B$ -values, whereas Cu is added for lower  $B$ -values [14]. The effects of Zn have been studied in spinel NTC ceramics [15–19]. It has been reported that, all of the Zn ions occupy the tetrahedral sites (A-sites) in spinel, and can improve the electrical stability effectively against processes and time [19]. But in almost all the published literatures [15–17], only the Mn element was partially replaced by other elements, because the amount of Mn ions is the key factor in the conductive process. However, not only the compositions can influence the electrical properties, but also the valence distribution of cations in different sites. The substituting of other cations besides Mn ions, may break the equilibrium of the distribution of Mn ions, which can also affect the electrical properties dramatically.

So in the present paper, the effects of substituting of Ni ions by Zn ions on the microstructure and electrical

F. Cheng · J. Wang · H. Zhang (✉) · A. Chang · W. Kong ·  
B. Zhang · L. Chen

Key Laboratory of Functional Materials and Devices under  
Special Environments of CAS, Xinjiang Key Laboratory of  
Electronic Information Materials and Devices, Xinjiang  
Technical Institute of Physics and Chemistry, CAS,  
Urumqi 830011, People's Republic of China  
e-mail: zhanghm@ms.xjb.ac.cn

F. Cheng · W. Kong · L. Chen  
University of Chinese Academy of Sciences, Beijing 100049,  
People's Republic of China

properties of  $\text{Ni}_{1-x}\text{Zn}_x\text{Mn}_2\text{O}_4$  ( $x = 0, 0.1, 0.2, 0.25, 0.4, 0.6, 0.8$ ) NTC ceramics were investigated, trying to prepare NTC thermistors with high stability.

## 2 Experimental

A series of  $\text{Ni}_{1-x}\text{Zn}_x\text{Mn}_2\text{O}_4$  ( $0 \leq x \leq 1$ ) NTC powders were prepared by the solid state reaction method. The NiO, ZnO and  $\text{Mn}_3\text{O}_4$  powder of analytical grade was weighed stoichiometrically as the raw materials. The as-weighed powder was mixed with alcohol and deionized water, and the mixture was ball-milled for 12 h using agate balls. The ball-milled slurries were dried at 90 °C, ground in mortar for 1 h and calcined at 900 °C for 3 h in alumina crucible, followed by grinding again. The ground powder was pressed at a pressure of 51 MPa to form a pellet of 10 mm in diameter. Subsequently, cold isostatic pressing at 300 MPa was used to enhance the green compacts' densities. The powder compacts covered by alumina powder, were sintered at 1,200 °C, then furnace-cooled to room temperature. The silver–palladium paste were spread on the two sides of the sintered pellets, and sintered at 835 °C for 20 mins.

The phase structures of the as-sintered ceramics were detected by X-ray diffraction (XRD; BRUKERD8-ADVANCE), using Cu  $K_\alpha$  radiation. The microstructure of the as-sintered ceramics was characterized by the Scanning electron microscope (SEM; LEO1430VP, Germany). The electrical resistivity of the  $\text{Ni}_{1-x}\text{Zn}_x\text{Mn}_2\text{O}_4$  NTC thermistors were measured by Agilent34970A multimeter in an oil bath. The complex impedance spectroscopy was obtained by an impedance analyzer (HP41494A) in a frequency range of 100 Hz–11 MHz, with different temperature (0, 25, 50, 80 °C). The drift of electrical resistivity at 25 °C was measured after aging test at 125 °C for 500 h.

## 3 Results and discussion

### 3.1 XRD

The results of XRD analysis of the  $\text{Ni}_{1-x}\text{Zn}_x\text{Mn}_2\text{O}_4$  ceramics sintered at 1,200 °C are shown in Fig. 1. For  $x = 0, 0.1, 0.2, 0.25$  and 0.4, the single cubic spinel phase was formed, and the lattice parameters were 8.3858, 8.3778, 8.3884, 8.3914 and 8.3867 nm, respectively. For  $x = 0.1, 0.2, 0.25$ , the lattice parameter increased with the increase of Zn content. These results should be attributed to the substitution of larger  $\text{Zn}^{2+}$  for  $\text{Ni}^{2+}$ , where the ionic radius of  $\text{Zn}^{2+}$  is 0.58 nm and that of  $\text{Ni}^{2+}$  is 0.565 nm [20]. Subsequently, the tetragonal spinel phase appeared firstly at  $x = 0.6$ . For  $0.6 \leq x \leq 0.8$ , the ceramics were

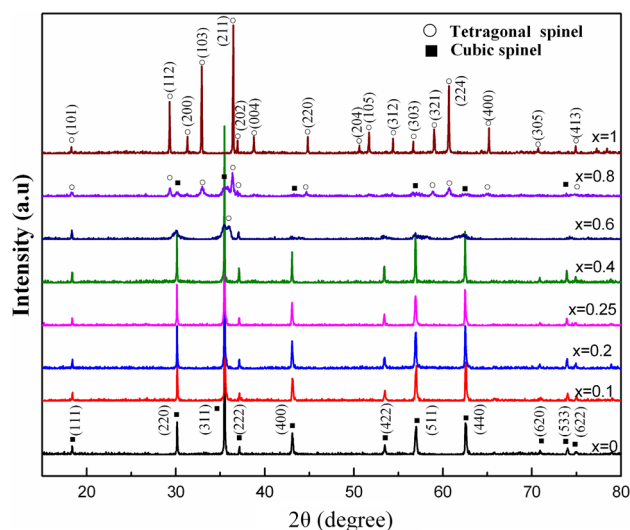


**Fig. 1** XRD patterns of the  $\text{Ni}_{1-x}\text{Zn}_x\text{Mn}_2\text{O}_4$  ( $0 \leq x \leq 1.0$ ) samples sintered at 1,200 °C

consisted of cubic spinel phase and tetragonal spinel phase. This indicates that the addition of Zn leads to the formation of tetragonal spinel phase. Finally, the single tetragonal spinel phase was formed for  $x = 1$ . Researches [21, 22] show that both  $\text{Ni}^{2+}$  and  $\text{Mn}^{2+}$  ions occupy the A-sites of  $\text{NiMn}_2\text{O}_4$  system, such as  $\text{Ni}_{1-x}^{2+}\text{Mn}_x^{2+}[\text{Ni}_v^{2+}\text{Mn}_{3+2v}^{4+}\text{O}_4^{2-}]$  model by Brabers et al. [22]. Because the  $\text{Zn}^{2+}$  cations prefer the A-sites in zinc manganite [23], the decreasing of Ni happens initially at A-sites then the B-sites with increasing Zn ions content. As a consequence, the  $\text{Mn}^{2+}$  in A-sites will transport to B-sites as  $\text{Mn}^{3+}$  when the Ni of B-sites decreases, which reduced the degree of inversion. When the concentration of  $\text{Mn}^{3+}$  in B-sites is large enough, the long range interaction of distorted octahedra results in a macroscopic tetragonal symmetry, as a result of the Jahn–Teller effect [1]. That's the reason why the phase structure changed with higher Zn ions content for  $\text{Ni}_{1-x}\text{Zn}_x\text{Mn}_2\text{O}_4$  ceramics.

### 3.2 SEM

The SEM images obtained from the surfaces of the as-sintered  $\text{Ni}_{1-x}\text{Zn}_x\text{Mn}_2\text{O}_4$  ( $0 \leq x \leq 0.8$ ) ceramics are shown in Fig. 2. With the SEM images, the range of grain sizes and the mean size of  $\text{Ni}_{1-x}\text{Zn}_x\text{Mn}_2\text{O}_4$  ( $0 \leq x \leq 0.8$ ) ceramics was calculated. The results are presented in Table 1. The mean grain sizes for  $x < 0.4$  are similar, but decreased obviously for  $x \geq 0.4$ . The density of the  $\text{Ni}_{1-x}\text{Zn}_x\text{Mn}_2\text{O}_4$  ( $0 \leq x \leq 1$ ) ceramics is shown in Table 2, measured by standard Archimedes method with distilled water. All the samples were of high density, ranging from 95.6 to 98.3 % of the theoretical density. More pores are observed in the SEM images for  $x = 0.6$  and 0.8. It shows

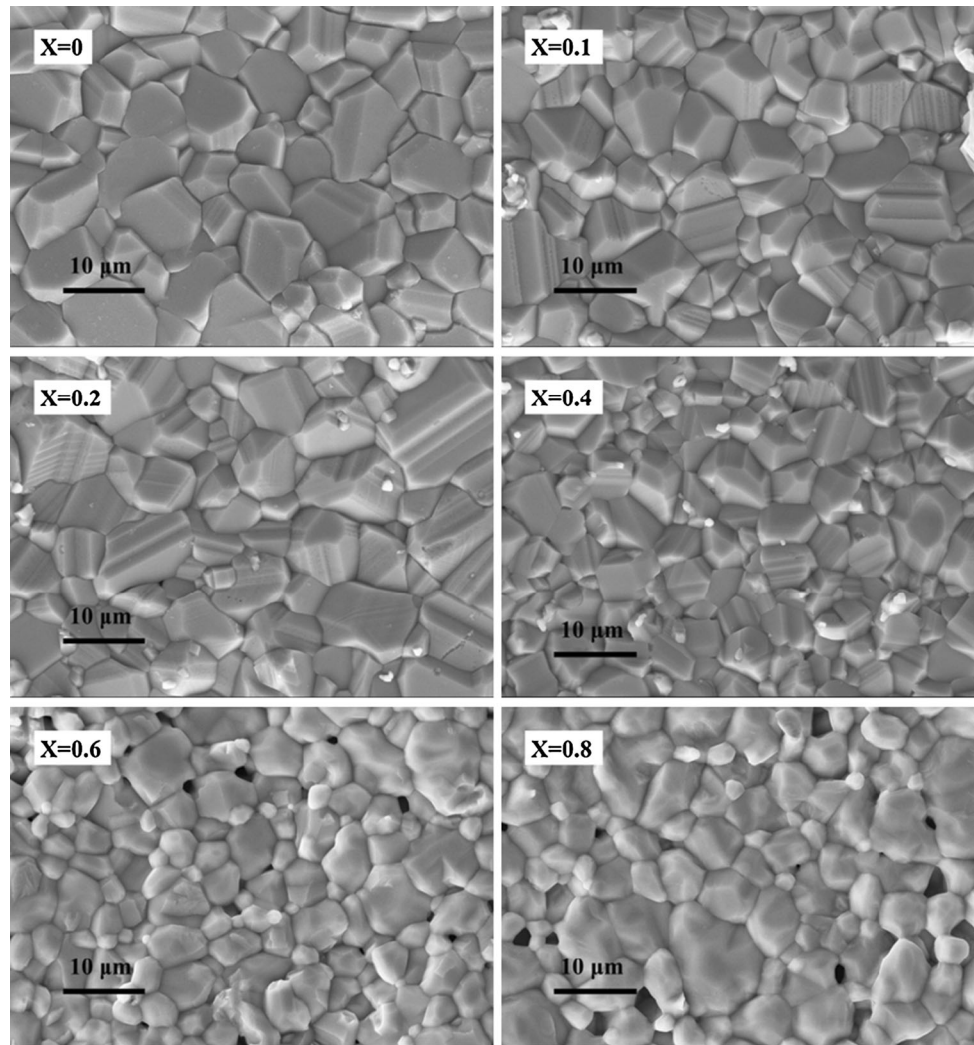


**Fig. 2** SEM images of the  $\text{Ni}_{1-x}\text{Zn}_x\text{Mn}_2\text{O}_4$  ( $0 \leq x \leq 0.8$ ) samples obtained from the surface of the samples sintered at 1,200 °C

**Table 1** The range of grain sizes and the mean grain sizes of  $\text{Ni}_{1-x}\text{Zn}_x\text{Mn}_2\text{O}_4$  ( $x = 0, 0.1, 0.2, 0.4, 0.6, 0.8$ ) ceramics

Samples	Range of grain sizes ( $\mu\text{m}$ )	Mean grain size ( $\mu\text{m}$ )
X = 0	2.02–10.09	5.49
X = 0.1	1.39–10.25	5.36
X = 0.2	1.41–13.89	5.68
X = 0.4	1.44–9.41	4.13
X = 0.6	1.16–10.59	4.10
X = 0.8	1.29–11.93	4.55

that the density for  $x = 0.6$  and  $0.8$  was lower than that of other samples, which was in accord with the measuring results. It indicates that the samples with single phase structure have higher density than the samples with complex phase structures. On the other hand, the shape of grains changed for different Zn ions content. The grains

**Table 2** The density of the  $\text{Ni}_{1-x}\text{Zn}_x\text{Mn}_2\text{O}_4$  ( $0 \leq x \leq 1$ ) ceramics

Samples	Density (%)	Samples	Density (%)
X = 0	97.3	X = 0.4	96.4
X = 0.1	96.8	X = 0.6	95.6
X = 0.2	97.1	X = 0.8	95.7
X = 0.25	96.3	X = 1	98.3

became not only smaller but also smoother for higher Zn content. What's more, polygonous grains and distinct grain boundaries existed in the ceramics for  $0 \leq x < 0.6$ , but the grain boundaries became vague for higher Zn ions content, and the grain had a trend to combine others to form a larger one, which was obvious in  $x = 0.8$ .

The change of the microstructure aforementioned can be explained by the phase transition. Stress can be induced in

grains of the ceramic while the transition from cubic to tetragonal spinel [1], which may originated from the difference of the thermal expansion coefficients of the two phases [15]. Because of the stress, the grains tend to shrink, which cause the emerging of pores and decreasing of grain size. The difference of microstructures will lead to the change of electrical properties of ceramics.

### 3.3 Electrical properties

The main electrical parameters of NTC thermistors are electrical resistivity ( $\rho$ ), relative resistance drift ( $\frac{\Delta R}{R_0}$ ) and material constant ( $B$ ) that represents the sensitivity of the materials. These parameters could be expressed as follows [24]:

$$\rho = \rho_0 \exp\left(\frac{E_a}{KT}\right), \tag{1}$$

$$\frac{\Delta R}{R_0} = \frac{R - R_0}{R_0}, \tag{2}$$

$$B_{25/50} = \frac{\ln(R_{25}/R_{50})}{1/T_{25} - 1/T_{50}}, \tag{3}$$

where  $\rho_0$  is the resistivity at infinite temperature,  $T$  is the absolute temperature,  $K$  is the Boltzmann constant and the  $E_a$  is the activation energy that can be calculated from the slope of the  $\ln \rho$  versus  $1/T$  plots.  $R_0$  and  $R$  are the resistance before and after ageing test.  $R_{25}$ ,  $R_{50}$  are the resistance measured at 25, 50 °C.

The relation between the natural logarithms of electrical resistivity ( $\ln \rho$ ) and the reciprocal of the absolute temperature ( $1/T$ ) of  $\text{Ni}_{1-x}\text{Zn}_x\text{Mn}_2\text{O}_4$  ( $0 \leq x \leq 0.8$ ) ceramics sintered at 1,200 °C are shown in Fig. 3. The relationship between  $\ln \rho$  and  $1/T$  of all the samples turned out to be linear, obeying the Eq. (1), which indicates that the as-sintered ceramics exhibited the typical characteristics of NTC thermistors. The electrical resistivity decreased slightly with the adding of Zn for  $0 \leq x < 0.4$  (part I), but increased dramatically for higher Zn content as  $x \geq 0.4$  (part II). As with part I, the  $\text{Mn}^{2+}$  in A-sites would transform to B-sites as  $\text{Mn}^{3+}$  gradually with the adding of Zn ions as mentioned before, so the amount of  $\text{Mn}^{3+}/\text{Mn}^{4+}$  pairs increased, which are essential to the electrical conductivity of Mn-based NTC thermistors [25]. That's the reason why the resistivity of the as-sintered ceramics decreased with higher  $x$  values in part I. The dramatic increase of electrical resistivity of the samples for part II may related to the change of microstructure and/or  $\text{Mn}^{3+}$  clustering in B-sites. On the one hand, samples for part II have smaller grains than part I, as shown in Table 1. It was reported that the decreased grain sizes would lead to the increase of resistivity [4, 26]. Because the smaller grains

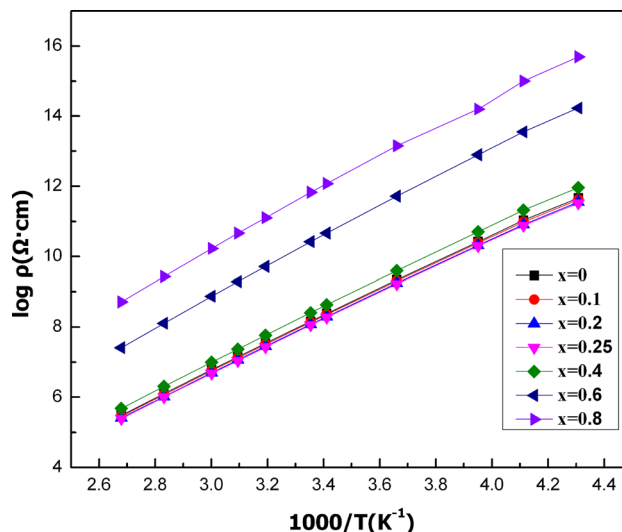


**Fig. 3** The relationship between the  $\log \rho$  and reciprocal of the absolute temperature for the  $\text{Ni}_{1-x}\text{Zn}_x\text{Mn}_2\text{O}_4$  ( $0 \leq x \leq 0.8$ ) samples sintered at 1,200 °C

**Table 3** The resistivity at 25 and 50 °C,  $B_{25/50}$  constant, and activity energy for  $\text{Ni}_{1-x}\text{Zn}_x\text{Mn}_2\text{O}_4$  ( $0 \leq x \leq 0.8$ ) NTC thermistors

Samples	$\rho_{25}$ ( $\Omega$ cm)	$\rho_{50}$ ( $\Omega$ cm)	$B_{25/50}$ (K)	Activity energy (eV)
X = 0	3,511	1,272	3,913	0.3291
X = 0.1	3,409	1,239	3,900	0.3277
X = 0.2	3,213	1,169	3,897	0.3271
X = 0.25	3,143	1,145	3,893	0.3265
X = 0.4	4,464	1,588	3,984	0.3347
X = 0.6	33,519	10,807	4,362	0.3630
X = 0.8	136,780	42,647	4,491	0.3691

shorten the time between the electron scattering events, increase the scattering frequency, and increased the resistivity. So the resistivity for part II was much larger than that for part I. On the other hand, in tetragonal spinel,  $\text{Mn}^{3+}$  with high concentration tend to cluster (gather themselves in a special direction), in order to reduce the lattices elastic energy [9]. These  $\text{Mn}^{3+}$  ions in cluster can no longer participate in the conduction because of the strong interaction between the  $\text{Mn}^{3+}$  ions, so that the resistivity increased with adding Zn for part II. The results show that the cubic structure is much more conductive than the tetragonal structure in spine. The similar results have been reported by Bordeneuve et al. [27]. As shown in Table 3, the values of  $\rho_{25}$ ,  $\rho_{50}$ ,  $B_{25/50}$  constant and activation energy  $E_a$  of the thermistors were in the range 3,511–136,780, 1,272–42,647  $\Omega$  cm, 3,913–4,491 K, and 0.3291–0.3691 eV, respectively. Some other works

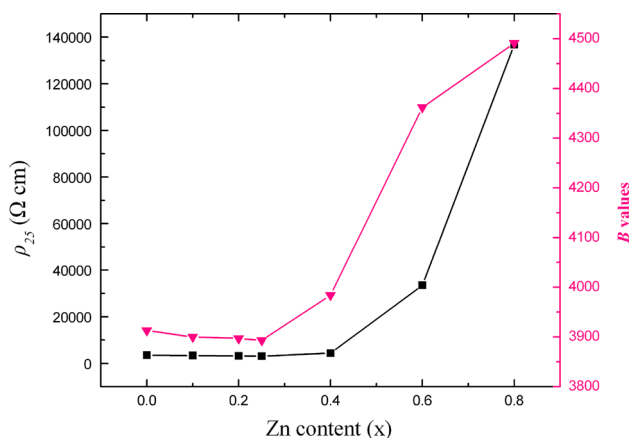


**Fig. 4** The  $\rho_{25}$  and  $B_{25/50}$  of  $\text{Ni}_{1-x}\text{Zn}_x\text{Mn}_2\text{O}_4$  ( $0 \leq x \leq 0.8$ ) NTC thermistors

concerning the similar compositions (Ni–Mn based) were reported by previous researchers. The range of room-temperature resistivity of different compositions varies for different composition, which decides the application temperature. For example, the  $\rho_{25}$  of  $\text{Ni}_{0.9}\text{Mn}_{2.1-x}\text{Si}_x\text{O}_4$  [28] ranged from 218 to 7,637  $\Omega$  cm, and that of  $\text{NiMn}_{2-x}\text{Zr}_x\text{O}_4$  [29] ranged from 89 to 1,153  $\Omega$  cm. Compared with  $\text{Ni}_{0.9}\text{Mn}_{2.1-x}\text{Si}_x\text{O}_4$  and  $\text{NiMn}_{2-x}\text{Zr}_x\text{O}_4$  systems, the  $\text{Ni}_{1-x}\text{Zn}_x\text{Mn}_2\text{O}_4$  ( $0 \leq x \leq 0.8$ ) ceramics have a larger and wider range of  $\rho_{25}$ . It indicates that the  $\text{Ni}_{1-x}\text{Zn}_x\text{Mn}_2\text{O}_4$  ( $0 \leq x \leq 0.8$ ) ceramics presents some complementary characteristics for Ni–Mn based NTC ceramics reported previously, and widens the application to higher temperature.

In order to reveal the relation between  $\rho_{25}$ ,  $B_{25/50}$  and Zn ions content clearly, Fig. 4 is presented. As shown in Fig. 4, the two lines have similar shapes, so that  $\rho_{25}$  and  $B_{25/50}$  of  $\text{Ni}_{1-x}\text{Zn}_x\text{Mn}_2\text{O}_4$  ceramics have the same tendency with increasing of Zn ions content. Both of the  $\rho_{25}$  and  $B_{25/50}$  have a minimum value at  $x = 0.25$ .

The relative resistance drifts for different compositions are shown in Fig. 5. The as-sintered  $\text{Ni}_{1-x}\text{Zn}_x\text{Mn}_2\text{O}_4$  ceramics exhibit a characteristic of relatively high stability. The relative resistance drift  $\Delta R/R_0$  was in the range of 0.69–1.72 % after aging test at 125 °C for 500 h. The maximum stability was obtained at  $x = 0.25$ , where  $\Delta R/R_0 = 0.69$  %. For  $x \leq 0.25$ , the introduction of Zn improved the thermal stability, in accordance with the results by Zhao and Zhao [17]. But for  $x > 0.25$ , the thermal stability deteriorated with increasing Zn content. The deterioration may be caused by the relatively lower density for  $x > 0.25$ , and it is believed that the higher density is beneficial to higher stability.

The lowest resistivity and highest stability were found at  $\text{Ni}_{0.75}\text{Zn}_{0.25}\text{Mn}_2\text{O}_4$  ceramic simultaneously, which indicate that the  $\text{Ni}_{0.75}\text{Zn}_{0.25}\text{Mn}_2\text{O}_4$  ceramic may have some

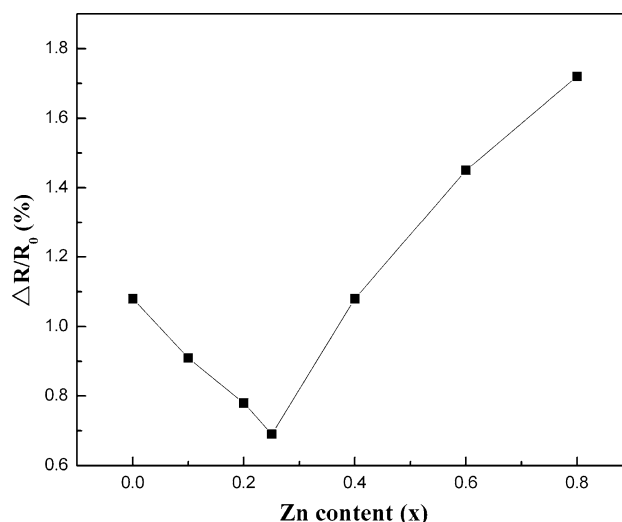


**Fig. 5** The relative resistance drift of  $\text{Ni}_{1-x}\text{Zn}_x\text{Mn}_2\text{O}_4$  ( $0 \leq x \leq 0.8$ ) NTC thermistors after ageing test at 125 °C for 500 h in air

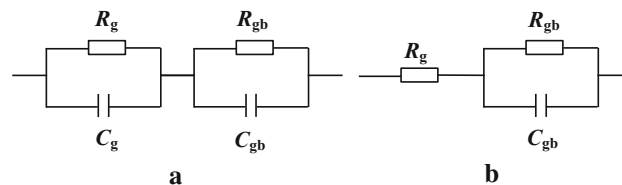


**Fig. 6** Equivalent circuits resulting from brick layer model

potential applications. Because of the adjustable wide range and high stability of resistivity and  $B$  values, the as-sintered  $\text{Ni}_{1-x}\text{Zn}_x\text{Mn}_2\text{O}_4$  ( $0 \leq x \leq 0.8$ ) ceramics would have a broad application as NTC thermistors.

#### 4 Complex impedance analysis

Complex impedance spectroscopy is an important way of characterizing the electrical properties of materials [30]. The equivalent circuit from the brick layer model [31] is shown in Fig. 6a. For many Mn-based NTC ceramics, the equivalent is usually simplified as Fig. 6b, because of the high resistance of grain boundaries [32, 33]. The relationship between the impedance spectrum and the resistance of grain and grain boundary can be expressed as follows [3]:

$$Z' = R_g + \left( \frac{R_{gb}}{1 + R_{gb}^2 C_{gb}^2 \omega^2} \right), \quad (4)$$

$$Z'' = \frac{R_{gb}^2 C_{gb} \omega}{1 + R_{gb}^2 C_{gb}^2 \omega^2}, \quad (5)$$

So the grain resistance ( $R_g$ ), sum of grain and grain boundaries resistance ( $R_g + R_{gb}$ ) could be obtained from



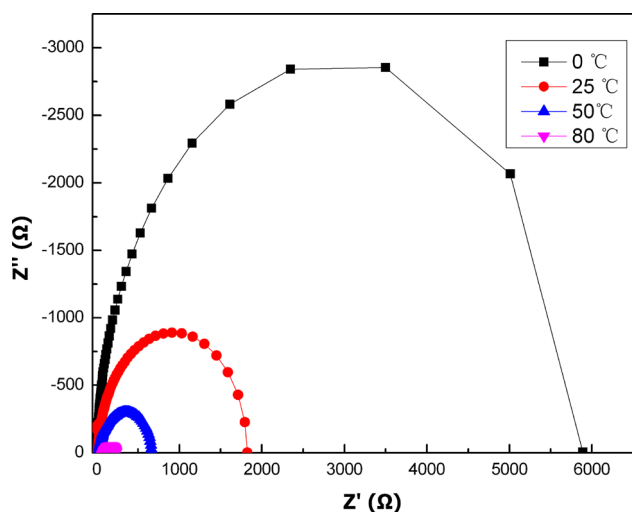


**Fig. 7** The complex impedance spectrum of  $\text{Ni}_{0.8}\text{Zn}_{0.2}\text{Mn}_2\text{O}_4$  sintered at 1,200 °C, with a range of temperature from 0 to 80 °C

the results of impedance analysis. The intercept of the semicircle and the real axis at lower frequencies is considered the value of  $(R_g + R_{gb})$ , and  $R_g$  could be obtained from the other intercept.

For  $\text{Ni}_{0.8}\text{Zn}_{0.2}\text{Mn}_2\text{O}_4$  ceramics, the relationships between  $R_g$ ,  $(R_g + R_{gb})$  and temperatures obtained from the impedance spectrum are shown in the Fig. 7. The  $R_{gb}$  decreased rapidly with increasing temperature, while the  $R_g$  almost unchanged. This indicates that the NTC characteristic of  $\text{Ni}_{0.8}\text{Zn}_{0.2}\text{Mn}_2\text{O}_4$  ceramics resulted from the change of  $R_{gb}$ .

The impedance spectrum of the  $\text{Ni}_{1-x}\text{Zn}_x\text{Mn}_2\text{O}_4$  ( $x = 0, 0.1, 0.2, 0.25, 0.4, 0.6, 0.8$ ) ceramics measured at 0 °C are presented as Fig. 8. The values of  $R_g$  and  $R_{gb}$  for different composition are shown in Table 4. The increase of resistance with adding of Zn for  $x > 0.25$  originate from the increase of grain boundary resistance  $R_{gb}$ . The increase of  $R_{gb}$  relates to the microstructure. It is reported that the grain boundary resistance is inversely proportional to  $\sqrt{n\alpha_{contact}}$ , where  $n$  is the number of grain-to-grain

contacts per grain, and  $\alpha_{contact}$  is the fraction of contacted area [34]. For porous ceramics ( $x > 0.25$ , as presented in the SEM images), both of the values of  $n$  and  $\alpha_{contact}$  decreased. As a result, the grain boundary resistance increased.

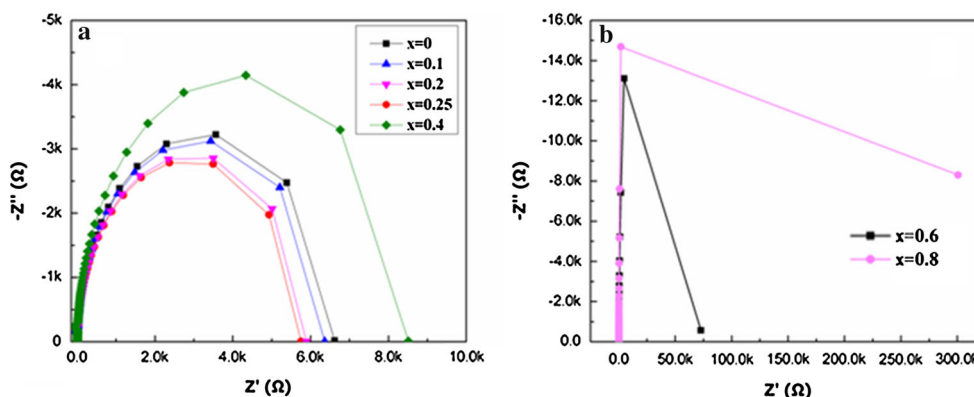
### 5 Conclusion

The properties of  $\text{Ni}_{1-x}\text{Zn}_x\text{Mn}_2\text{O}_4$  ( $0 \leq x \leq 1$ ) ceramics could be tuned effectively, because the substituting changed the valance distribution of cations, which is essential for conduction. The phase composition turned out to be single cubic spinel for  $0 \leq x \leq 0.4$ , tetragonal phase coexisted for  $0.6 \leq x \leq 0.8$ , and single tetragonal phase for  $x = 1$ . The resistivity decreased slightly with the increase of Zn ions content for  $0 \leq x \leq 0.25$ , but increased dramatically for higher Zn ions content for  $x > 0.25$  due to the  $\text{Mn}^{3+}$  clustering and/or the change of microstructure. The values of  $\rho_{25}$ ,  $B_{25/50}$  constant and activation energy for  $\text{Ni}_{1-x}\text{Zn}_x\text{Mn}_2\text{O}_4$  ( $0 \leq x \leq 0.8$ ) NTC thermistors were in the range 3,511–136,780 Ω cm, 3,913–4,491 K and 0.3265–0.3691 eV, respectively. The as-prepared thermistors exhibit a characteristic of high thermal stability that the relative resistance drift for  $0 \leq x \leq 0.8$  was in the range of 0.69–1.72 % after aging test for 500 h. The maximum stability and lowest resistivity was obtained at

**Table 4** The values of  $R_g$  and  $R_{gb}$  of  $\text{Ni}_{1-x}\text{Zn}_x\text{Mn}_2\text{O}_4$  ( $0 \leq x \leq 0.8$ ) ceramics measured at 0 °C

Samples	$R_g$	$R_{gb}$
X = 0	7.4379	6608.4221
X = 0.1	7.1944	6351.3256
X = 0.2	7.5109	5882.3115
X = 0.25	7.6626	5745.5074
X = 0.4	7.1973	8504.9527
X = 0.6	5.6652	73391.2348
X = 0.8	4.6800	300573.3200

**Fig. 8** The complex impedance spectrum of  $\text{Ni}_{1-x}\text{Zn}_x\text{Mn}_2\text{O}_4$  ( $0 \leq x \leq 0.8$ ) samples measured at 0 °C



$x = 0.25$ , which indicate that the  $\text{Ni}_{0.75}\text{Zn}_{0.25}\text{Mn}_2\text{O}_4$  is an interesting composition. These results reveal that the substituting of Ni by Zn have various effects for different phase structures.

**Acknowledgments** This work was supported by the National High Technology Research and Development Program of China (No. 2012AA091102), and West Light Foundation of Chinese Academy of Science (No. XBBS201314).

## References

1. A. Feteira, J. Am. Ceram. Soc. **92**, 967 (2009)
2. W. Zhou, L. Zhang, C. Ouyang, J. Wu, Z. Huang, Appl. Surf. Sci. **311**, 443 (2014)
3. B. Zhang, Q. Zhao, A. Chang, J. Yao, P. Zhao, F. Guan, W. Kong, J. Alloy. Compd. **512**, 132 (2012)
4. K. Park, J.K. Lee, S.J. Kim, J. Korean Phys. Soc. **49**, 585 (2006)
5. J. Wang, J. Yao, Z. Chen, Y. Fan, A. Chang, D. Jia, J. Mater. Sci. Mater. Electron. **24**, 622 (2013)
6. M.N. Muralidharan, P.R. Rohini, E.K. Sunny, K.R. Dayas, A. Seema, Ceram. Int. **38**, 6481 (2012)
7. L. He, Z.Y. Ling, Y.T. Huang, Y.S. Liu, Mater. Lett. **65**, 1632 (2011)
8. B. Zhang, Q. Zhao, A. Chang, Y. Li, Y. Liu, Y. Wu, Appl. Phys. Lett. **104**, 102 (2014)
9. K. Fujiwara, S. Lee, N. Donnelly, T. Yamaguchi, C.A. Randall, J. Am. Ceram. Soc. **92**, 2634 (2009)
10. J. Wang, J. Zhang, J. Mater. Res. **27**, 928 (2012)
11. G.D.C. Csete de Györgyfalva, I.M. Reaney, J. Eur. Ceram. Soc. **21**, 2145 (2001)
12. Y. Chang-Lai, L. Ying, Z. Xiu-Juan et al., J. Inorg. Mater. **29**, 91 (2014)
13. C. Peng, H. Zhang, A. Chang, F. Guan, B. Zhang, P. Zhao, J. Mater. Sci. Mater. Electron. **23**, 851 (2012)
14. A. Feteira, K. Reichmann, Adv. Sci. Technol. **67**, 124 (2011)
15. K. Park, J.K. Lee, S.J. Kim, W.S. Seo, W.S. Cho, C.W. Lee, S. Nahm, J. Alloy. Compd. **467**, 310 (2009)
16. C. Zhao, B. Wang, P. Yang, L. Winnubest, C. Chen, J. Eur. Ceram. Soc. **28**, 35 (2008)
17. C. Zhao, Y. Zhao, J. Mater. Sci. Mater. Electron. **23**, 1788 (2012)
18. O.S. Aleksic, M.V. Nikolic, M.D. Lukovic, N. Nikolica, B.M. Radojicib, M. Radovanovic, Z. Djuricd, M. Mitrice, P.M. Nikolic, Mater. Sci. Eng. B **178**, 202 (2013)
19. C. Zhao, Y. Zhao, Y. Wang, Solid State Commun. **152**, 593 (2012)
20. H.S.C. O'Neill, A. Navrotsky, Am. Mineral. **68**, 181 (1983)
21. E.D. Macklen, J. Phys. Chem. Solids **47**, 1073 (1986)
22. V.A.M. Brabers, F.M. Van Setten, P.S.A. Knapen, J. Solid State Chem. **49**, 93 (1983)
23. C. Chanel, S. Fritsch, C. Drouet, A. Rousseta, M.L. Martinez Sarriónb, L. Mestresb, M. Moralesb, Mater. Res. Bull. **35**, 431 (2000)
24. M.A.L. Nobre, S. Lanfredi, Appl. Phys. Lett. **81**, 451 (2002)
25. S.E. Dorris, T.O. Mason, J. Am. Ceram. Soc. **71**, 379 (1988)
26. K. Park, D.Y. Bang, J. Korean Phys. Soc. **41**, 251 (2002)
27. H. Bordeneuve, S. Guillemet-Fritsch, A. Rousset, C. Tenailleau, S. Guillemet-Fritsch, J. Solid State Chem. **182**, 396 (2009)
28. K. Park, S.J. Yun, J. Mater. Sci. Mater. Electron. **15**, 359 (2004)
29. K. Park, Mater. Sci. Eng. B **104**, 9 (2003)
30. E. Barsoukov, J.R. Macdonald, *Impedance Spectroscopy Theory, Experiment, and Applications*, 2nd edn. (Wiley, New Jersey, 2005), pp. 1–2
31. J.E. Bauerle, J. Phys. Chem. Solid **30**, 2657 (1969)
32. S.G. Song, Z. Ling, F. Placido, Mater. Res. Bull. **40**, 1081 (2005)
33. W. Kong, L. Chen, B. Gao, B. Zhang, P. Zhao, G. Ji, A. Chang, C. Jiang, Ceram. Int. **40**, 8405 (2014)
34. J. Fleig, J. Maier, J. Eur. Ceram. Soc. **19**, 693 (1999)